25. E. Apra *et al.*, NWChem, version 4.7 (Pacific Northwest National Laboratory, Richland, WA, 2005).
26. D. R. Hamann, *Phys. Rev. B* **40**, 2980 (1989).
27. L. Kleinman, D. M. Bylander, *Phys. Rev. Lett.* **48**, 1425 (1982).
28. J. P. Perdew, K. Burke, M. Ernzerhof, *Phys. Rev. Lett.* **77**, 3865 (1996).
29. Materials and methods are available as supporting material on *Science* Online.
30. M. C. Cruickshank, L. S. Dent Glasser, S. A. I. Barri, I. J. F. Poplett, *J. Chem. Soc. Chem. Commun.* **23**, 23 (1986).
31. B. C. Faust *et al.*, *Geochim. Cosmochim. Acta* **59**, 2651 (1995).
32. L-O. Öhman, *Geochim. Cosmochim. Acta* **61**, 3257 (1997).
33. D. A. Palmer, D. J. Wesolowski, *Geochim. Cosmochim. Acta* **57**, 2929 (1993).
34. We thank J. Weare for helping to develop the simulations. The research was supported by separate grants from the Office of Basic Energy Science of the U.S. Department of Energy to W.H.C. and E.B., from the U.S. NSF to B.L.P. and W.H.C., and from the Natural Sciences and Engineering Research Council of Canada to T.W.S.

An Observation of PKJKP: Inferences on Inner Core Shear Properties

Aimin Cao,[1]* Barbara Romanowicz,[1] Nozomu Takeuchi[2]

The seismic phase PKJKP, which traverses the inner core as a shear wave and would provide direct evidence for its solidity, has been difficult to detect. Using stacked broadband records from the Gräfenberg array in Germany, we documented a high signal-to-noise phase, the arrival time and slowness of which agree with theoretical predictions for PKJKP. The back azimuth of this arrival is also consistent with predictions for PKJKP, as is the comparison with a pseudoliquid inner core model. Envelope modeling of the PKJKP waveform implies a shear velocity gradient with depth in the inner core that is slightly larger than that in the preliminary reference Earth model.

Soon after Lehmann (*1*) discovered Earth's inner core in 1936 through the analysis of travel times of teleseismic body waves, Birch (*2*) suggested that the inner core should be solid as a result of freezing of liquid iron. Thirty years later, indirect evidence of the solidity of the inner core was documented by means of seismic normal mode eigenfrequency measurements (*3*). However, the observation of the phase PKJKP, which traverses the inner core as a shear wave (Fig. 1A), has been a controversial issue. Julian *et al.* (*4*) and Okal and Cansi (*5*) each suggested the detection of PKJKP on the basis of data from short-period seismic arrays at frequencies of ~1.0 Hz and 0.1 to 0.5 Hz, respectively. Deuss *et al.* (*6*) argued that these two claims were misidentifications, and instead proposed an observation of pPKJKP+SKJKP between 0.01 and 0.1 Hz.

PKIKP, which traverses the inner core as a compressional wave (Fig. 1A), is routinely observed. It should be observed simultaneously with PKJKP in the epicentral distance range 116° to 180°, according to the seismic preliminary reference Earth model (PREM) (*7*). The relative amplitude of PKJKP varies strongly with frequency (Fig. 1B). Although we cannot rule out the possibility of observing PKJKP at frequencies of 0.1 to 0.5 Hz (*5*), it is more likely to be found at lower frequencies (*6*).

Here, we used data from the broadband Gräfenberg Seismic Array (GRF) in Germany to detect PKJKP (Fig. 1C). With an aperture of ~100 × 50 km, GRF has provided continuous records at 13 stations since 1980. Its location with respect to frequent large events (moment magnitude $M_w > 7.0$) in the south Pacific Ocean at distances of ~140° makes it an ideal broadband seismic array to study PKJKP. We studied ~20 large events in the vicinity of Tonga and Santa Cruz islands occurring from 1980 to 1999 (*8*). One of the events ($M_w = 7.3$, depth = 76 km, 6 February 1999) is uniquely favorable to the observation of PKJKP (Fig. 1C). We chose the band measuring 0.06 to 0.1 Hz for our analysis (*9*).

We aligned the seismograms with respect to the origin time of the event and made an array-sided travel time correction (fig. S1A) (*10*), filtered the data with a band-pass filter, normalized the seismograms with respect to the first arrival (PKIKP+PKiKP), and stacked them using the phase-weighted stack (PWS) technique (*11*). We computed two vespagrams. The first one (Fig. 2A) corresponds to the time and slowness window within which we expect to find the group PKIKP/PKiKP and their depth phases. The second one (Fig. 2C) corresponds to the predicted window for PKJKP, according to the PREM model (*7*). We observe clear energy maxima in both windows. We also observe a clean stacked waveform corresponding to the energy maximum in the PKJKP window (Fig. 2D). We verified that this phase arrives within 5° of the great circle path from the source, ruling out a scattered near-array phase (Fig. 2E).

We further investigated whether this phase could be a mantle, outer core, or even crust phase, by considering for reference a model with a liquid inner core, as was done by Deuss *et al.* (*6*). In such a model, there would not be a PKJKP phase. We constructed synthetic vespagrams using the direct-solution method (DSM) (*12, 13*).

Consideration of near source local structure, as well as moment tensor information (*13*) allowed us to model both the waveform of PKIKP+PKiKP and its depth phase, pPKIKP+pPKiKP (Fig. 3A) for both solid and liquid inner cores, providing accurate source-time functions for the synthetic calculations. It is not possible to discern PKJKP in an individual synthetic trace, because PKJKP is so weak that it is deeply hidden behind unidentifiable mantle, outer core, and crust phases. To extract the PKJKP phase, we generated synthetic differential seismograms between solid inner core and liquid inner core (Fig. 3B). However, even when we chose a shear-wave quality factor $Q_\beta = 300$ for the solid inner core, PKJKP and pPKJKP were not prominent enough. This is because transmission coefficients of the inner core *P*-wave phases (PcPPKIKP, pPcPPKIKP, sPcPPKIKP, and PKKPdf; fig. S4) are artificially increased in the case of the liquid inner core, compared with the real earth. This artificial energy is weak, but stronger than that of the potential PKJKP.

The liquid inner core model serves to remove the inner core shear-wave energy from the time window shown in Fig. 3B, so as to better extract PKJKP and pPKJKP in the differential seismogram. We can also achieve this by reducing the shear-wave velocity in the inner core by 8% compared with the PREM model. In this case, the inner core shear-wave energy moves beyond the appropriate time window (PKJKP and pPKJKP are moved backward by ~50 s). Meanwhile, the artificial compressional energy is considerably reduced (Fig. 3C) and both PKJKP and pPKJKP phases are present in the synthetic differential seismogram. pPKJKP is ~2.2 times as weak as PKJKP. If we also take the background noise into account, the amplitude ratio of PKJKP to pPKJKP may be as large as ~4.8 (fig. S2). Therefore, it is not surprising that we do not observe pPKJKP for this event. We thus only discuss PKJKP. Synthetic vespagrams for this pseudoliquid inner core (Fig. 4A) show that there is no energy maximum corresponding to waves with negative slowness, confirming that the target phase observed in Fig. 2, C, D, and E, is not a crust, mantle, or outer core phase (*14*).

[1]Seismological Laboratory, University of California, Berkeley. [2]Earthquake Research Institute, University of Tokyo, Japan.

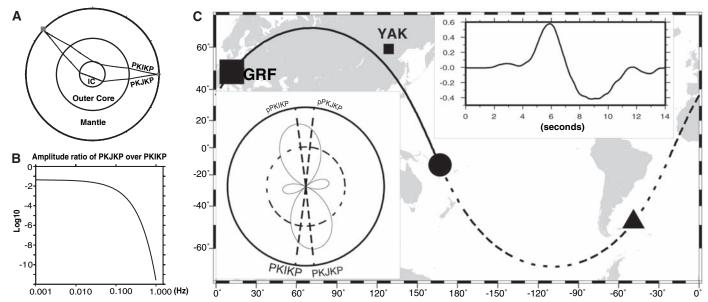*To whom correspondence should be addressed. E-mail: acao@seismo.berkeley.edu

Fig. 1. (**A**) Ray paths of PKJKP and PKIKP. The point on the right and square on the left indicate the source and GRF array locations, respectively. IC, inner core. (**B**) The theoretical amplitude ratio of PKJKP over PKIKP as a function of frequency based on the reference model PREM (7), after correcting for transmission and geometrical spreading (16). The reference epicentral distance is 138°. Given the dynamic range of present seismometers, it is unlikely that one could observe PKJKP (or pPKJKP) in the frequency range ~1.0 Hz (4). (**C**) Geographical setting of the event (dot) and GRF seismic array (square). The solid line is the ray path of PKIKP and the dashed line is the ray path of PKJKP projected on Earth's surface. The triangle marks the location of the bottoming point of PKJKP in the inner core. The upper right inset shows the source-time history of the event characterized by a P phase recorded at a broadband station (YAK, distance = 80.1°) of the Global Seismographic Network, located in a similar azimuth as GRF. The lower left inset illustrates the P-wave radiation pattern in the vertical plane of the great circle. This event is exceptional: (i) The source duration is less than 9 s; (ii) the expected PKJKP is emitted from the top of the lobe of the P-wave radiation pattern; and (iii) the potential interfering phases identified in previous studies (4, 5), such as PcPPKIKP, pPcPPKIKP, sPcPPKIKP, and PKKPdf, are at least 17 s away from the predicted PKJKP arrival time (according to PREM).
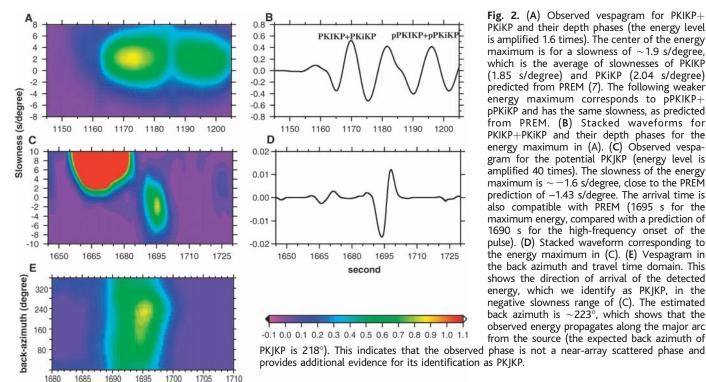

Fig. 2. (**A**) Observed vespagram for PKIKP+ PKiKP and their depth phases (the energy level is amplified 1.6 times). The center of the energy maximum is for a slowness of ~1.9 s/degree, which is the average of slownesses of PKIKP (1.85 s/degree) and PKiKP (2.04 s/degree) predicted from PREM (7). The following weaker energy maximum corresponds to pPKIKP+ pPKiKP and has the same slowness, as predicted from PREM. (**B**) Stacked waveforms for PKIKP+PKiKP and their depth phases for the energy maximum in (A). (**C**) Observed vespagram for the potential PKJKP (energy level is amplified 40 times). The slowness of the energy maximum is ~−1.6 s/degree, close to the PREM prediction of −1.43 s/degree. The arrival time is also compatible with PREM (1695 s for the maximum energy, compared with a prediction of 1690 s for the high-frequency onset of the pulse). (**D**) Stacked waveform corresponding to the energy maximum in (C). (**E**) Vespagram in the back azimuth and travel time domain. This shows the direction of arrival of the detected energy, which we identify as PKJKP, in the negative slowness range of (C). The estimated back azimuth is ~223°, which shows that the observed energy propagates along the major arc from the source (the expected back azimuth of PKJKP is 218°). This indicates that the observed phase is not a near-array scattered phase and provides additional evidence for its identification as PKJKP.

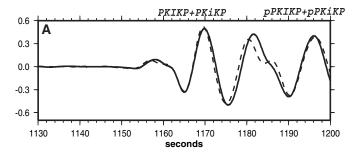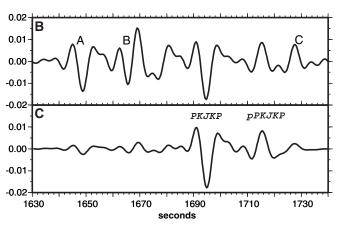The PKJKP waveform (Fig. 2D) allows us to estimate the shear-wave velocity in the inner core by envelope-function modeling. Synthetic envelope functions of PKJKP are computed from the synthetic differential seismograms between the solid inner core and the pseudoliquid inner core (13). We process the synthetic differential seismograms in the same way as the observed seismogram and compare the envelope with the observed one (fig. S2). The envelope-function modeling suggests that the observed PKJKP is about 9.0 s faster than the

Fig. 3. Synthetic modeling. (**A**) Waveform modeling of PKIKP+PKiKP as well as pPKIKP+pPKiKP based on U.S. Geological Survey Preliminary Determination of Epicenters moment tensor. Both the observed (dashed line) and the synthetic (solid line) seismograms are normalized after applying the band-pass filter (0.06 to 0.1 Hz). Synthetics are obtained with DSM (*12*). (**B**) Synthetic differential seismogram for the PREM model compared with a true liquid inner core, for which the shear-wave velocity is equal to zero. A (PcPPKIKP), B (pPcPPKIKP+sPcPPKIKP), and C (PKKPdf) are artificially enhanced by the assumption of liquid inner core. (**C**) Synthetic differential seismogram based on the pseudoliquid inner core

used in this Report. We now can clearly see both PKJKP and pPKJKP phases. The amplitude of PKJKP is approximately 2.2 times as large as that of pPKJKP.
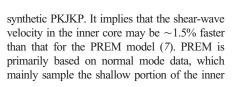
Fig. 4. Synthetic vespagrams. (**A**) Pseudoliquid inner core model. Time windows are identical to those in Fig. 2C. Energy level is amplified 40 times, as in Fig. 2C. D, E, and F are crust, mantle, or outer core phases, and G is PcPPKIKP. See fig. S3 for a plot with energy level amplified only 20 times to bring out the relative strength of these phases. (**B**) Solid inner core model, assuming $Q_\beta = 300$. Because the strong mantle phase E in the synthetic model arrives at the same time as PKJKP, the dominant energy of phase E hides the much weaker PKJKP, which only slightly distorts the pattern of phase E. Likewise, pPKJKP slightly distorts the pattern of phase F. Phases E and F are not present in the observed stacks. Therefore, we cannot directly use the comparison of observed vespagram to that predicted by the solid inner core model; instead, we use a differential seismogram modeling approach, in which the energy from phases E and F is removed. (**C**) Synthetic differential vespagram in the slowness-time domain. This vespagram is calculated for the solid inner core minus the pseudoliquid inner core models. The time window is the same as that in Fig. 3C. The estimated slownesses of the energy maxima are both −1.4 s/degree, as are the predictions based on PREM. This identifies the two phases in the differential seismogram (Fig. 3C) as PKJKP and pPKJKP.

synthetic PKJKP. It implies that the shear-wave velocity in the inner core may be ~1.5% faster than that for the PREM model (*7*). PREM is primarily based on normal mode data, which mainly sample the shallow portion of the inner core, whereas here, PKJKP samples the central part (Fig. 1A). Thus, it is in agreement with previous results if one allows for a slight increase in shear velocity with depth in the inner core. The use of GRF array data was key to this study (*15*).

References and Notes

1. I. Lehmann, *Bur. Centr. Seismol. Int. A.* **14**, 87 (1936).
2. F. Birch, *Am. J. Sci.* **238**, 192 (1940).
3. A. M. Dziewonski, F. Gilbert, *Nature* **234**, 465 (1971).
4. B. R. Julian, D. Davies, R. M. Sheppard, *Nature* **235**, 317 (1972).
5. E. A. Okal, Y. Cansi, *Earth Planet. Sci. Lett.* **164**, 23 (1998).
6. A. Deuss, J. H. Woodhouse, H. Paulssen, J. Trampert, *Geophys. J. Int.* **142**, 67 (2000).
7. A. M. Dziewonski, D. L. Anderson, *Phys. Earth Planet. Inter.* **25**, 297 (1981).
8. The relocated catalog by Engdahl *et al.* is available for this time period; E. R. Engdahl, R. D. van der Hilst, R. P. Buland, *Bull. Seismol. Soc. Am.* **88**, 722 (1998).
9. From 100 s before PKIKP and 200 s after PKJKP, the amplitude spectrum (fig. S1B) indicates that the amplitude decays significantly at periods longer than 0.06 Hz. Only in the frequency range 0.06 to 0.1 Hz is the amplitude relatively constant.
10. The GRF seismic array has a relatively small aperture, but there is still noticeable variation of differential travel times of PKIKP, which can be as large as 0.6 s across the array. This variation is presumed to be primarily related to crust and/or uppermost mantle heterogeneity just beneath the array. This heterogeneity should also influence PKJKP at a similar level, because the two ray paths are very close in this region (Fig. 1A). GRB2, which is at the center of this broadband seismic array, is chosen as the reference station.
11. M. Schimmel, H. Paulssen, *Geophys. J. Int.* **130**, 497 (1997).
12. N. Takeuchi, R. J. Geller, P. R. Cummins, *Geophys. Res. Lett.* **23**, 1175 (1996).
13. Materials and methods are available as supporting material on *Science* Online.
14. The phase observed in Fig. 2, C and D, cannot be due to random noise. (i) The PWS stacking technique (*11*) is designed specifically to remove the influence of the background incoherent noise. (ii) If what we observed had been random noise, the energy extrema should have also distributed randomly in the observed vespagram.
15. Compared with global broadband seismic networks (*6*), GRF has a number of distinct advantages: (i) We can examine all potential interfering phases, which are expected to appear in the time window of our study, to make sure they arrive sufficiently far away in time and/or slowness from PKJKP. When global networks are used, the number of identifiable interfering phases is much larger. As a result, it seems more difficult to prevent the relatively strong phase(s) from appearing close to PKJKP (or pPKJKP). Usually, the stacking technique cannot suppress this kind of energy completely and thus cannot prevent these phases from interfering with the very weak PKJKP (or pPKJKP) energy (*11*). (ii) We can expect that the presumed PKJKP phases recorded at every station in GRF are coherent. When using global networks, one must correct for polarities of the expected PKJKP (or pPKJKP) phases in different quadrants if they are opposite. (iii) GRF stations use identical seismometers. We can directly process the data without removing instrument responses as we adopt normalized traces to constrain Q_β. Although the aperture of GRF seismic array is relatively small for this very sharp large event, it is sensitive to small perturbations in arrival times (as low as ~0.3 s) using vespagrams. This is also the reason that the array-sided travel time correction is necessary.
16. A. Cao, B. Romanowicz, *Earth Planet. Sci. Lett.* **228**, 243 (2004).
17. We thank the Gräfenberg Array operators for the long-term high-quality maintenance of their array. This work was supported by NSF grant EAR-0308750. This is Berkeley Seismological Laboratory contribution 05-08.